J Nanostruct 16(2): 2607-2615, Spring 2026

RESEARCH PAPER

$TiO_2/BiDyO_3$ Nanocomposite for Visible-Light Driven Photocatalytic Degradation of Acid Blue 113

Amenah Radhi Hamad [1], Zuhra Muter Saleh Al_bakity [2], Doaa Abbood Challoob [3]*

[1] The General Directorate of Misan Education, Ministry of Education, Iraq
[2] Department of Chemistry, College of Science, University of Misan, Misan, Iraq
[3] The General Directorate of Misan Education, Ministry of Education, Iraq

ARTICLE INFO

Article History:
Received 04 December 2025
Accepted 24 March 2026
Published 01 April 2026

Keywords:
Acid blue 113
Nanocomposite
Photocatalyst
$TiO_2/BiDyO_3$
Visible light

ABSTRACT

$TiO_2/BiDyO_3$ (TiO_2/BDO) nanocomposite was synthesized as efficient photocatalyst to drive degradation of acid blue 113 (AB113) solution under visible light irradiation. Optical characterization strongly confirmed the excellent visible-light photoactivity. Incorporation of $BiDyO_3$ into TiO_2 network led to a reduction in band gap value (2.57 eV) and also improved separation of charge carriers. Photocatalytic reactions were conducted for 180 min using the nanocomposites incorporated with different concentrations of $BiDyO_3$. The highest degradation efficiency was achieved using the nanocomposite containing 6%wt of $BiDyO_3$ nanoparticles (TiO_2/6-BDO). Experiments performed to identify the optimum loading amount of the nanocomposite revealed that the 0.05 g of the TiO_2/6-BDO provides the best AB113 degradation results. Due to anionic nature of AB113, positively charged surface of the nanocomposite under acidic pH favored achieving the improved degradation efficiency. In addition, the H_2O_2 oxidant (1 mL, 0.01 M) enhanced degradation efficiency of AB113. Reusability of the nanocomposite was tested through six reaction cycles, showing the great photocatalytic stability.

How to cite this article
Radhi Hamad A., Saleh Al_bakity Z., Abbood Challoob D. $TiO_2/BiDyO_3$ Nanocomposite for Visible-Light Driven Photocatalytic Degradation of Acid Blue 113. J Nanostruct, 2026; 16(2):2607-2615. DOI: 10.22052/JNS.2026.02.099

INTRODUCTION

With advent of photocatalysis, wastewater treatment has witnessed tremendous developments that increases the hope to overcome environmental crises in the near future [1-3]. Oceans and seas all over the world are contaminated with toxic and persistent organic pollutants from industrial zones, farms and cities [4, 5]. As a result, emerging diseases are becoming prevalent, and health agencies have to spend large sum of money to treat these newly occurred diseases [6, 7]. Additionally, fighting with environmental crises stemming from water pollution requires billions of dollars, and developing countries need much more international supports in this regard [8, 9].

Photocatalysis is a new technology for removing organic pollutants from water media, which offers several advantages with respect to conventional treatment methods [10-12]. Photocatalysis is based on advanced oxidation processes, utilizing the photo-induced generation of oxidative species to mineralize pollutants [13]. Based on this, photocatalysis is considered as

* *Corresponding Author Email: Zuhra91@uomisan.edu.iq*

This work is licensed under the Creative Commons Attribution 4.0 International License.
To view a copy of this license, visit http://creativecommons.org/licenses/by/4.0/.

an environmentally friendly approach due to elimination of toxic chemicals used in conventional methods [14, 15]. Moreover, photocatalysis treatment is powerful enough to completely degrade persistent pollutants without generating dangerous intermediates [16].

Despite aforesaid advantages, the photocatalytic method suffers from some obstacles that largely limit its efficiency [17]. In this regard, the poor activation of common photocatalyst materials, including titanium dioxide (TiO_2) and zinc oxide (ZnO), under visible light irradiation is significant limitation, hindering the widespread utilization of photocatalysis [18]. Consequently, numerous efforts have been devoted to exploiting the visible light spectrum for conducting photocatalytic reactions. In this context, nanocomposite materials benefit from synergistic electronic interactions between components, which effectively enhance the visible light activity of photocatalysts [19].

For examples, Saadati et al. reported synthesis of $TiO_{2-x}/FeTiO_3$ heterojunction photocatalyst for degradation of organic pollutants under the visible light irradiation [20]. Fatima et al. synthesized $Yb_2O_3/ZnFe_2O_4$ nanocomposite for photocatalytic degradation of dye and herbicide [21]. Also, a binary nanocomposite comprising $WO_3/CeTiO_4$ has been synthesized for solar activated photocatalytic degradation of reactive orange 30 [22].

In this work, $TiO_2/BiDyO_3$ nanocomposite (TiO_2/BDO) was synthesized as a highly efficient visible light driven photocatalyst for degradation of organic pollutant. Aqueous solution of acid blue 113 (AB113) was used to examine the photocatalytic activity of the nanocomposite. Various parameters were investigated to study the efficiency of TiO_2/BDO nanocomposite for removal of pollutants under different conditions.

MATERIALS AND METHODS

Synthesis of $BiDyO_3$ nanoparticles

$BiDyO_3$ (BDO) nanoparticles were synthesized by a co-precipitation method in an aqueous medium. The required nitrate precursors, $Bi(NO_3)_3.5H_2O$ and $Dy(NO_3)_3.5H_2O$, were dissolved in water and mixed to obtain a homogeneous precursor solution.

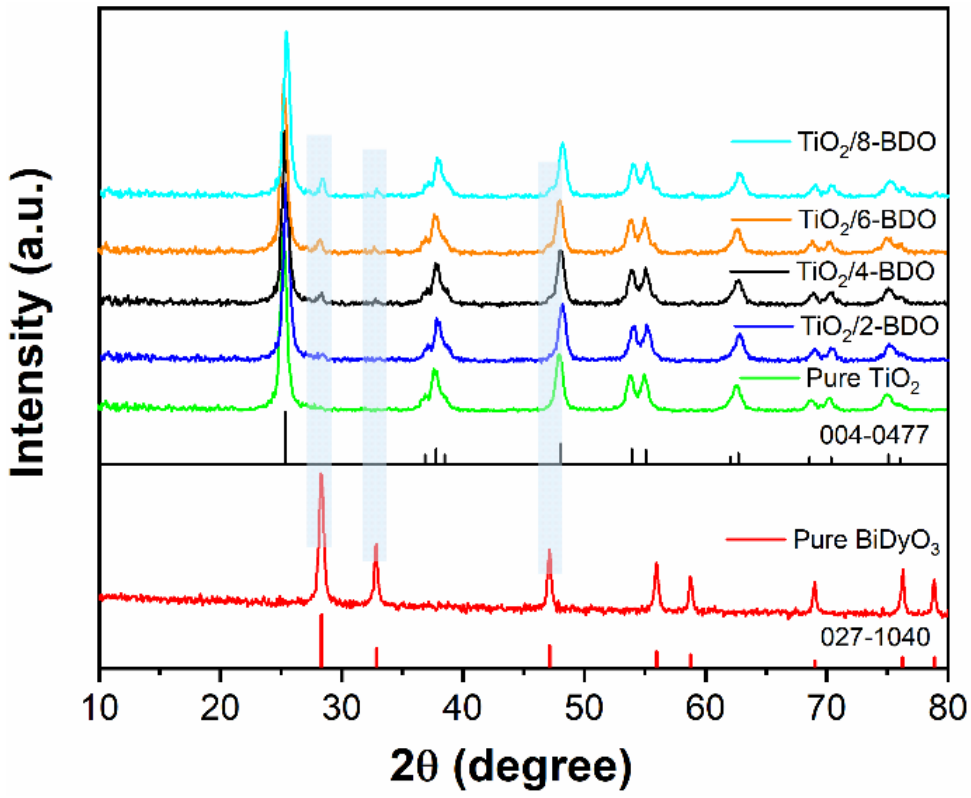


Fig. 1. XRD patterns for the synthesized samples.

Polyethylene glycol was used as a capping agent to influence particle growth of the precipitated solid. NH_4OH solution (0.5 M) was then added gradually under continuous mixing until the solution reached neutral pH and precipitation reaction was completed. The solid was collected and washed with water and ethanol to remove soluble residual species. The washed solid was dried at 100 °C and subsequently calcined at 800 °C for 7 h to promote formation and crystallization of the BDO nanoparticles.

Synthesis of TiO_2 nanoparticles

The TiO_2 nanoparticles were synthesized by a sol–gel route. Absolute ethanol was used as the reaction medium, followed by addition of a small amount of citric acid and ethylene glycol. Tetrabutyl orthotitanate (TBOT) was then introduced under mixing. The solution was maintained under mild heating in an oven at 60 °C until the sol gradually transformed into a gel. Further heating was applied to obtain a dry gel. The dried gel was finally calcined at 600 °C for 3 h to produce the pure TiO_2 nanoparticles.

Synthesis of TiO_2/$BiDyO_3$ nanocomposite

The TiO_2/BDO nanocomposites were synthesized by adding as-prepared BDO nanoparticles to the TiO_2 sol at the amounts 2, 4, 6, and 8 wt.%. The BDO nanoparticles were dispersed into the TiO_2 sol under identical preparation conditions for each composition. The resulting mixtures were dried and calcined under the same conditions, yielding TiO_2/2-DBO, TiO_2/4-DBO, TiO_2/6-DBO, and TiO_2/8-DBO.

Characterization

X-ray diffraction (XRD) (Philips X'pert pro MPD) was used to identify crystalline phases and evaluate the structural characteristics and crystallinity of the synthesized nanocomposites. Field emission scanning electron microscopy (FESEM) (TESCAN mira 3) was used to examine particle morphology and surface features. Diffuse reflectance spectroscopy (DRS) (JASCO UV-Vis) was used to investigate optical absorption and the visible-light response of the samples. Photoluminescence (PL) spectroscopy (CARY ECLIPSE) was used to compare the recombination behavior of photogenerated charge carriers among the prepared nanocomposites.

Photocatalytic experiments

The Photocatalytic degradation processes were performed using 50 mL of an aqueous Acid Blue 113 (AB113) solution with an initial concentration of 50 ppm. The visible light irradiation was supplied by an LED lamp (100 W, white color) from the fixed distance of 30 cm, and the irradiation period was carried out at the interval time of 180 min. Before illumination, the AB113 solution containing the TiO_2/BDO nanocomposite was stirred in the dark to establish adsorption equilibrium. The AB113 concentration was subsequently monitored during irradiation by UV–visible spectroscopy. The influence of nanocomposite loading amounts was

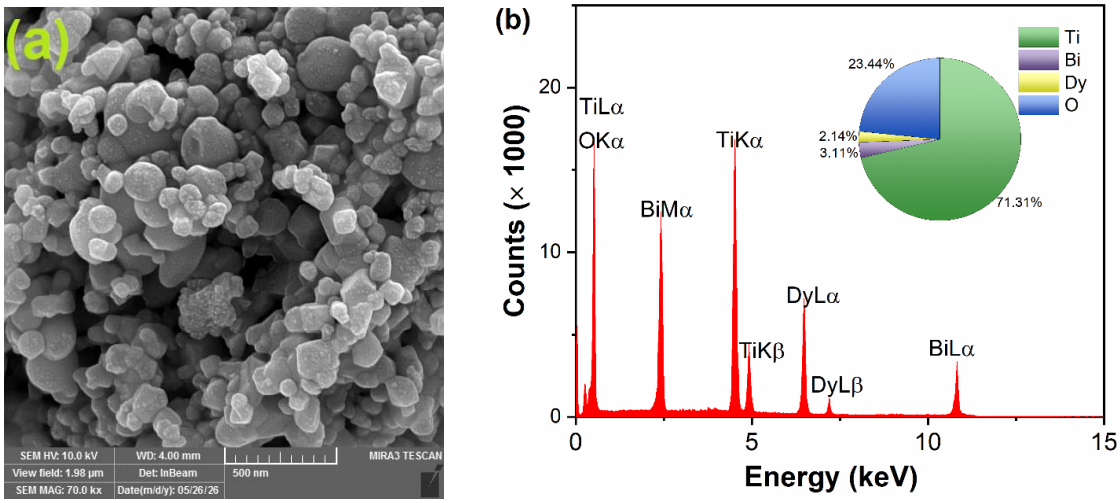


Fig. 2. FESEM image (a) and EDX spectrum (b) of TiO_2/6-BDO nanocomposite.

CC BY

examined using 0.01, 0.02, 0.03, 0.04, and 0.05 g of the nanocomposite. The initial pH was adjusted to 3, 5, 7, 9, or 11. The effect of H_2O_2 was investigated at concentrations of 0.01, 0.02, and 0.03 M.

RESULTS AND DISCUSSION

XRD, FESEM, DRS, and PL results

Fig. 1 exhibits the XRD patterns of the TiO_2/x-BDO nanocomposites containing different concentrations of DBO nanoparticles. The observed pattern for the $BiDyO_3$ (BDO) nanoparticles clearly matches with the JCPDS reference code (027-1040) for the cubic structure of bismuth dysprosium oxide. Also, the synthesized TiO_2 shows the pattern corresponds to the anatase phase of titanium dioxide (JCPDS code: 004-0477). As can be seen form the Fig. 1, the incorporation of BDO into the TiO_2 matrix brings two diffraction peaks at 2Θ around 28° and 32°, which are intensified as the BDO concentration increases. Also, a shoulder can be observed at around 47°, which is attributed to the BDO phase.

The FESEM image in Fig. 2a illustrates the morphological features of the TiO_2/6-BDO nanocomposite. The quasi-spherical particles in the size range around 100 nm are clearly observed. In addition, the EDX spectrum (Fig. 2b) revealed the composition of the nanocomposite, including Ti (71.31%), Bi (3.11%), Dy (2.14%), and O (23.44%).

The optical properties of the synthesized nanocomposite were analyzed using DRS and PL spectroscopy. Fig. 3a shows the DRS spectra for the pure TiO_2 and TiO_2/x-BDO nanocomposites. As clearly observed, the light absorption in the visible region improved with increasing the concentration of BDO. The TiO_2/6-BDO nanocomposite possesses the significant visible light absorption,

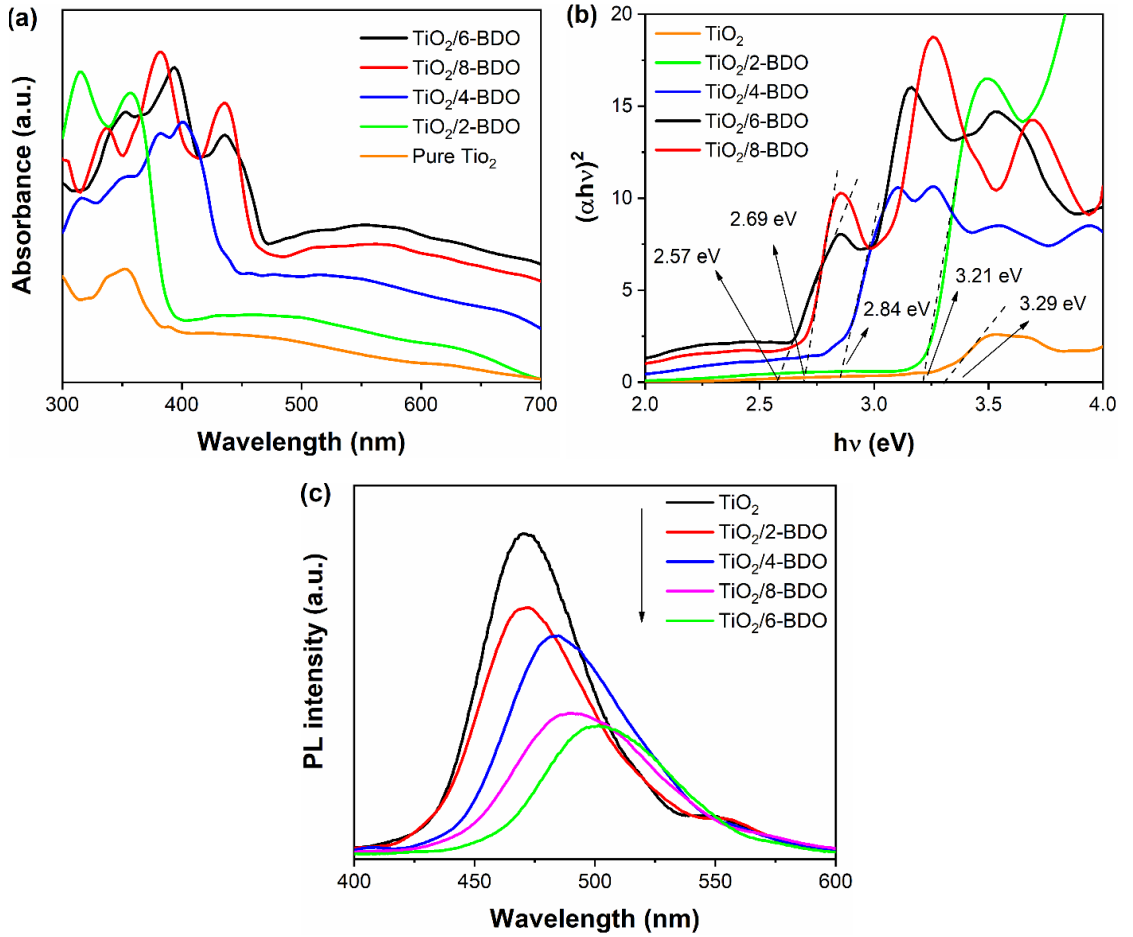


Fig. 3. DRS spectra (a), Tauc plots (b), and PL spectra (c) of the TiO_2/x-BDO nanocomposites.

while incorporation of 8 wt% of BDO into the TiO_2 network led to slight decrease in the visible light characteristic. One the most important features observed in DRS spectra is the absorption edge, which shifted to the longer wavelengths when the BDO content increased. The optical band gap for the nanocomposites was calculated by plotting $(\alpha hv)^2$ with respect to hv and extrapolating the linear portion of the curves to the hv axis [23]. The results showed that the band gap values were 3.29, 3.21, 2.84, 2.57, and 2.69 eV for the pure TiO_2, TiO_2/2-BDO, TiO_2/4-BDO, TiO_2/6-BDO, and TiO_2/8-BDO, respectively.

Furthermore, the PL spectra in Fig. 3b provide further information on the optical properties of the TiO_2/x-BDO nanocomposites. Given that the photoluminescence originates from returning the excited electrons to the ground states, the PL intensity is directly associated to the effectiveness of accomplished mechanisms to retard the recombination of the electron-hole pairs [24]. In this regard, the pure TiO_2 represents the strong PL peaks, revealing the fast recombination of the photo-generated electrons and holes. The incorporation of the BDO into the TiO_2 matrix forms the new energy levels that facilitate the electron transfer, thereby decreasing the recombination rate of the charge carriers [25, 26]. As seen, the TiO_2/6-BDO nanocomposite shows the lowest PL intensity, confirming the improved separation of charge carriers and the photocatalytic activity. However, the nanocomposite containing 8 wt% of the BDO nanoparticles has the slight increase in the PL intensity compared with the TiO_2/6-BDO nanocomposite.

Photocatalytic activity of TiO_2/x-BDO nanocomposites

The visible light photocatalytic activity of the pure TiO_2 and the TiO_2/DBO nanocomposites was first compared at the fixed photocatalyst amount of 0.04 g. Fig. 4 shows after 180 min of the photocatalytic reaction, the pure TiO_2 produced only 16.83% degradation of AB113. Incorporation of 2 wt% BDO nanoparticles increased the degradation to 49.11%. Increasing the BDO content to 4 wt% raised the removal efficiency of the AB113 to 89.92%, while TiO_2/6BDO

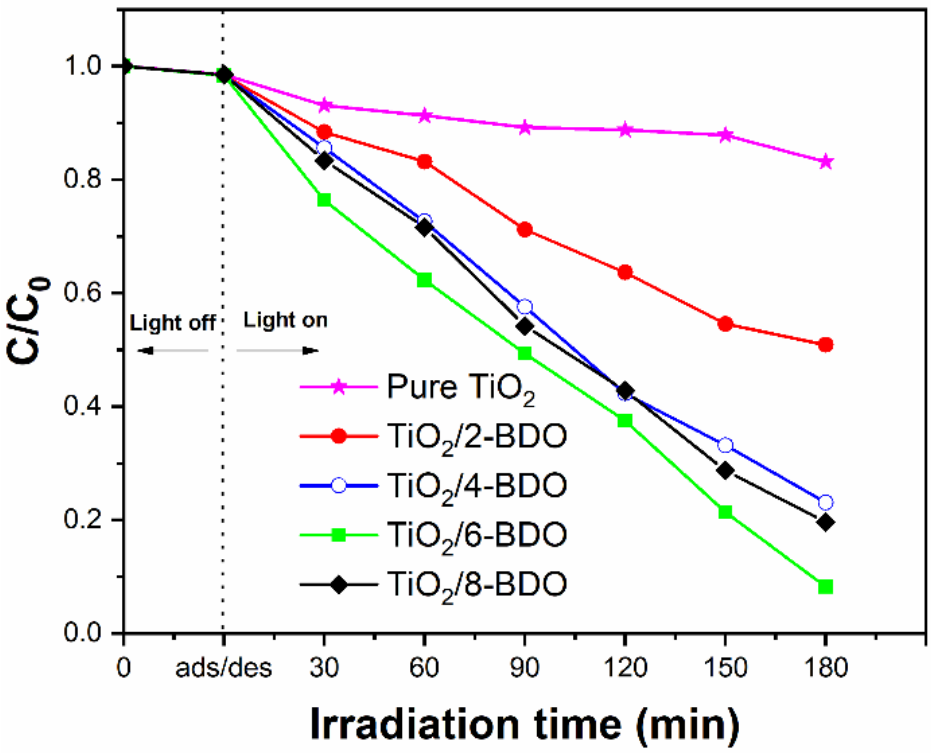


Fig. 4. Photocatalytic performance of TiO_2/x-BDO nanocomposites for degradation of AB113.

CC BY

nanocomposite reached 91.77%. Further addition of BDO nanoparticles to 8 wt% caused the efficiency to decline to 80.35%.

The marked improvement after coupling BDO nanoparticles with TiO_2 indicates that the BDO has the beneficial role in visible-light photocatalysis. Formation of the new energy levels can provide a pathway for photogenerated charge migration between the two components, resulting in the improved separation of electron–hole pairs [27]. These electronic interactions also enhance the utilization of the visible light irradiation, which was

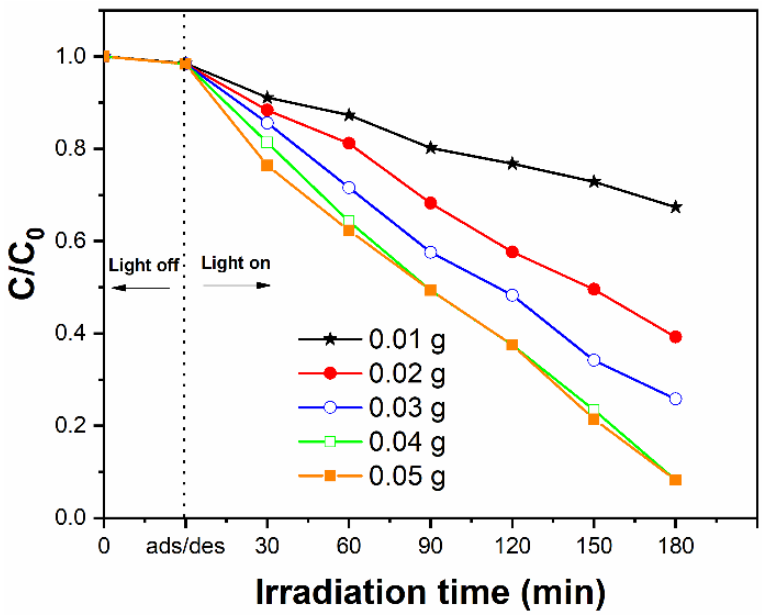


Fig. 5. Photocatalytic degradation of AB113 using different amounts of TiO_2/6-BDO nanocomposite.

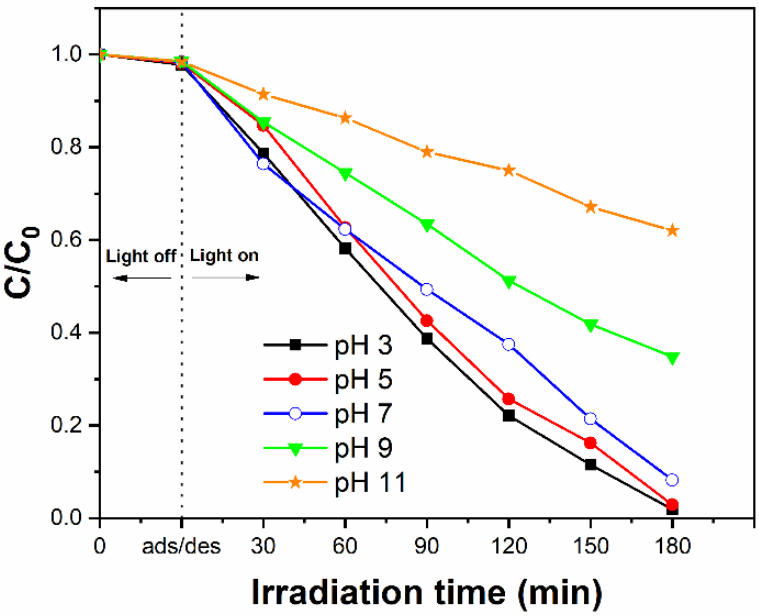


Fig. 6. Photocatalytic degradation of AB113 under different pH conditions.

CC BY

confirmed by PL and DRS results (Fig. 3). However, the decline observed at 8 wt% suggests that the amount of the second phase must be optimized. Excess BDO nanoparticles may cover active TiO_2 sites, alter the accessibility of the interface, increase light scattering, or introduce defect sites that facilitate charge loss.

Different loading amounts of TiO_2/6-BDO nanocomposite

Fig. 5 shows the photodegradation of the AB113 solution using different amounts of the TiO_2/6-BDO nanocomposite. As can be seen, 0.01 g of the TiO_2/6-BDO nanocomposite produced 32.61% degradation efficiency after 180 min. In addition,

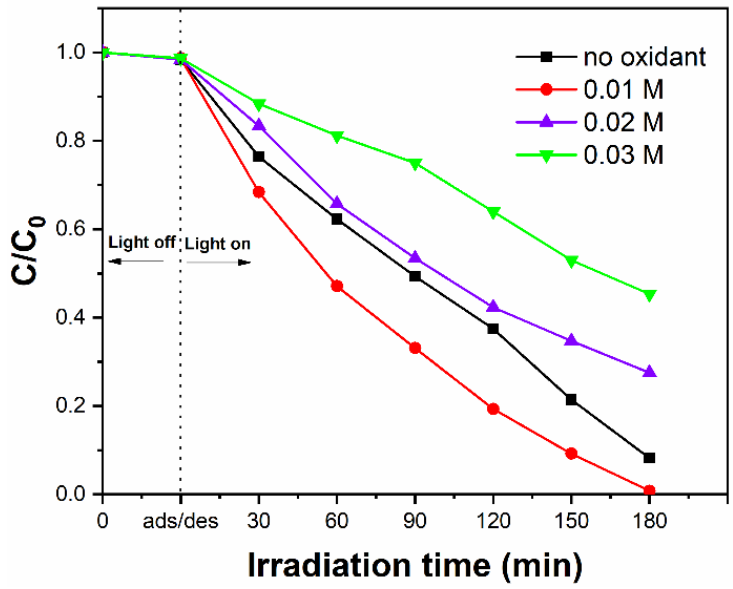


Fig. 7. Photocatalytic degradation of AB113 in the presence of different concentrations of H_2O_2.

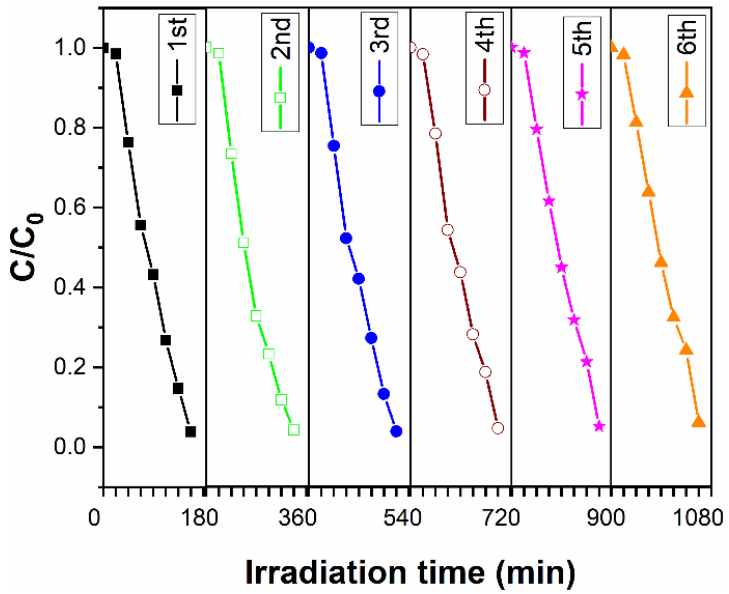


Fig. 8. Reusability experiments for the TiO_2/6-BDO nanocomposite.

CC BY

the gradual increase in the photocatalytic efficiency was provided using increasing the amount of the nanocomposite. The highest removal of AB113 was approximately 96.12%, which was obtained with 0.05 g of the TiO_2/6-BDO nanocomposite. The observed enhancement in the photocatalytic activity is attributed to the greater number of available active surface sites upon addition of more amount of the nanocomposite [28, 29]. The increased number of active sites imply that the more AB113 molecules can adsorb on the surface of the nanocomposite and then degrade using generated radicals.

Different pH of AB113

Electrostatic interaction between the AB113 molecules and the TiO_2/6-BDO surface is particularly important. Hence, the effect of AB113 solution pH on the photocatalytic efficiency was studied. As shown in Fig. 6, the degradation efficiency at pH 3 reached approximately 98%, which was slightly higher than the degradation results obtained pH 7 (96%). However, the significant reductions in the photocatalytic activity were observed at pH 9 and 11.

Due to negative charge of AB113 molecules [30], their adsorption on the active surface sites of the nanocomposite is higher at acidic conditions compared to that of under alkaline pHs [31, 32]. At lower pH, the surface of the nanocomposite is protonated and carries positive charges, which can electrostatically interact with the AB113 molecules. However, under alkaline conditions, de-protonation of surface groups can increase the negative character of the nanocomposite, increasing the electrostatic repulsion between the negatively charged surface and the anionic dye.

Different concentrations of H_2O_2

H_2O_2 was introduced as an auxiliary oxidant to promote the visible-light photocatalysis for removal of AB113. The H_2O_2 concentration was varied from 0.01 to 0.03 M and its effect was investigated on the removal efficiency of AB113 using the TiO_2/6-BDO nanocomposite, as shown in Fig. 7. The results showed that increasing the H_2O_2 concentration initially improved AB113 degradation, with the best performance obtained at 0.01 M and degradation approaching complete removal. The improvement can be associated with the ability of H_2O_2 to participate in the generation of highly reactive radical species and thereby provide additional oxidation levels [33]. However, the benefit did not continue indefinitely. At 0.02 and 0.03 M, the degradation decreased, indicating that excessive H_2O_2 interferes with the radical production [34].

Reusability of nanocomposite

The reusability of the TiO_2/6-BDO nanocomposite was evaluated over six consecutive photocatalytic cycles. After each cycle, the nanocomposite was recovered using centrifugation at 5500 rpm for 5 min, washed with water and ethanol, dried, and reused under the same reaction conditions. Fig. 8 shows the reusability results for the degradation of AB113 using 0.5 g of the TiO_2/6-BDO nanocomposite. As can be seen, the nanocomposite maintained the high level of activity throughout the repeated tests. However, after the sixth cycle, the degradation efficiency decreased by approximately 2.27%, which is attributed to the gradual loss of the nanocomposite during recovery, washing, and transfer between cycles. Overall, the degradation efficiency remained unchanged through the third cycle, indicating good stability of the synthesized TiO_2/6-BDO nanocomposite under repeated operation.

CONCLUSION

In conclusion, the $TiO_2/BiDyO_3$ (TiO_2/BDO) nanocomposite showed good potential for the photocatalytic degradation of AB113 under visible light. The results indicates that the addition of $BiDyO_3$ to TiO_2 improved the potential properties of the nanocomposite by decreasing the band gap to 2.57 eV and enhancing the separation of charge carriers. Among the synthesized samples, TiO_2/6-BDO showed the highest photocatalytic activity. It was also found that 0.05 g of this nanocomposite was the optimum photocatalyst amount for AB113 degradation. The degradation process was more effective under acidic conditions, which can be related to the positively charged surface of the nanocomposite and its favorable interaction with the anionic AB113 molecules. The presence of H_2O_2 also increased the degradation efficiency. Furthermore, the photocatalyst showed good stability after six consecutive cycles, confirming its potential for repeated use. These results suggest that the synthesized TiO_2/6-BDO nanocomposite can be effectively used for the degradation of AB113 in the visible-light-driven photocatalytic

CC BY

processes.

CONFLICT OF INTEREST

The authors declare that there is no conflict of interests regarding the publication of this manuscript.

REFERENCES

1. Ariza Gonzalez M, Hoijang S, Tran DB, Tran QM, Atik R, Islam R, et al. Surface-Modified Magnetic Nanoparticles for Photocatalytic Degradation of Antibiotics in Wastewater: A Review. Applied Sciences. 2026;16(2):844.
2. Xu Y, Chiam SL, Leo CP, Hu Z. Recent Advances in Photocatalytic TiO_2-based Membranes for Eliminating Water Pollutants. Separation and Purification Reviews. 2025;55(2):150-167.
3. Swamy KR, Shyamala G, Gurugubelli TR, Ravindran G, Bathula B. Recent advancements of wastewater treatment by photocatalysis: A comprehensive review. iScience. 2026;29(6):116088.
4. Yuan F, Wei YD, Gao J, Chen W. Water crisis, environmental regulations and location dynamics of pollution-intensive industries in China: A study of the Taihu Lake watershed. Journal of Cleaner Production. 2019;216:311-322.
5. Rathour RK, Sakhuja D, Bhatt AK, Bhatia RK. Municipal Wastewater Connection for Water Crisis and Jaundice Outbreaks in Shimla City: Present Findings and Future Solutions. International Journal of Environmental Research and Public Health. 2022;19(18):11266.
6. Karak P, Parveen A, Modak A, Adhikari A, Chakrabortty S. Microplastic Pollution: A Global Environmental Crisis Impacting Marine Life, Human Health, and Potential Innovative Sustainable Solutions. International Journal of Environmental Research and Public Health. 2025;22(6):889.
7. Demir E, Kacew S. Relationships Between Environmental Toxicology and Human Health. Int J Mol Sci. 2026;27(5):2399.
8. Kathuria V. Controlling water pollution in developing and transition countries—lessons from three successful cases. J Environ Manage. 2006;78(4):405-426.
9. Price JI, Heberling MT. The Effects of Source Water Quality on Drinking Water Treatment Costs: A Review and Synthesis of Empirical Literature. Ecol Econ. 2018;151:195-209.
10. Khan S, Noor T, Iqbal N, Yaqoob L. Photocatalytic Dye Degradation from Textile Wastewater: A Review. ACS Omega. 2024;9(20):21751-21767.
11. Rauf MA, Ashraf SS. Fundamental principles and application of heterogeneous photocatalytic degradation of dyes in solution. Chem Eng J. 2009;151(1-3):10-18.
12. Afridi SK, Umar K, Razali MR, Raza W. Photocatalytic Degradation of Pesticides Employing Metal-doped and Graphene-interfaced Semiconductor Nanocomposites: Advantages, Mechanism and Affecting Parameters. Water, Air, and Soil Pollution. 2026;237(15).
13. Patel V, Kumar V, Indra A. Single-Atom Cocatalyst-Loaded Semiconductors for Photo-Fenton-Like Wastewater Treatment. Chemistry – An Asian Journal. 2026;21(6).
14. Li Q, Zhang Z, Wang Z, Zhou H, Zhao F, Wei T, et al. Atomic level surface on aluminum alloy produced by novel environmentally-friendly photocatalytic chemical mechanical polishing with high material removal rate using hybrid ceria nanoabrasives. Tribology International. 2026;221:112080.
15. El-Fawal EM, El Naggar AMA, El Sayed HA, El-Zahhar AA, Alghamdi MM, Soliman FS. Production of environmentally-friendly diesel fuel through designation of polystyrene-based hybrid nanocomposites for efficient photocatalytic desulfurization. Journal of Environmental Chemical Engineering. 2026;14(2):122144.
16. Daghrir R, Drogui P, Robert D. Modified TiO_2 For Environmental Photocatalytic Applications: A Review. Industrial and Engineering Chemistry Research. 2013;52(10):3581-3599.
17. Anwer H, Mahmood A, Lee J, Kim K-H, Park J-W, Yip ACK. Photocatalysts for degradation of dyes in industrial effluents: Opportunities and challenges. Nano Research. 2019;12(5):955-972.
18. Sapkal RT, Shinde SS, Mahadik MA, Mohite VS, Waghmode TR, Govindwar SP, et al. Photoelectrocatalytic decolorization and degradation of textile effluent using ZnO thin films. J Photochem Photobiol B: Biol. 2012;114:102-107.
19. Wang S, Yun J-H, Luo B, Butburee T, Peerakiatkhajohn P, Thaweesak S, et al. Recent Progress on Visible Light Responsive Heterojunctions for Photocatalytic Applications. Journal of Materials Science and Technology. 2017;33(1):1-22.
20. Saadati A, Habibi-Yangjeh A, Khataee A. A facile synthesis of S-scheme TiO_{2-x}/$FeTiO_3$ heterojunction photocatalyst for multifunctional hazardous pollutants degradation. J Alloys Compd. 2026;1063:187150.
21. Fatima N, Dwivedi S, Bansal P, Veg E, Mishra V, Khan T. Environmental applications of an ultrasonically synthesized and PEG assisted Yb_2O_3/$ZnFe_2O_4$ nanocomposite for dye and herbicide degradation and electrochemical sensing of catechol. Dalton Transactions. 2026;55(5):2200-2223.
22. Vasithira E, Archunan S, Silambarasan J, Dharmaraja J, Krishnaveni A, Sivakumar S, et al. Enhanced Photocatalytic Degradation of Reactive Orange 30 Using WO3/CeTiO4 Binary Nanocomposites with Band Gap Engineering and Superior Solar-Driven Efficiency. Waste and Biomass Valorization. 2025;17(1):31-43.
23. Escobedo-Morales A, Pedraza-Chan MS, Ruiz-López II, Anota EC, Salazar-Villanueva M, Cortés-Arriagada D. Accurate determination of the band gap energy of non-translucent semiconductor materials through the Tauc method: Theoretical framework, limitations, technical hints, and automated algorithms. Next Materials. 2026;10:101412.
24. Rahbar M, Hosseini-Sarvari M. Natural sunlight-driven photocatalytic mineralization of petrochemical wastewater using ceramic-supported Fe, B co-doped TiO_2/CNT@WO_3 in a flat panel photoreactor. Journal of Water Process Engineering. 2025;77:108328.
25. Nosaka Y, Nosaka AY. Generation and Detection of Reactive Oxygen Species in Photocatalysis. Chem Rev. 2017;117(17):11302-11336.
26. Wang H, Zhang L, Chen Z, Hu J, Li S, Wang Z, et al. Semiconductor heterojunction photocatalysts: design, construction, and photocatalytic performances. Chem Soc Rev. 2014;43(15):5234.
27. Low J, Yu J, Jaroniec M, Wageh S, Al-Ghamdi AA. Heterojunction Photocatalysts. Adv Mater. 2017;29(20).
28. Pelaez M, Nolan NT, Pillai SC, Seery MK, Falaras P, Kontos AG, et al. A review on the visible light active titanium dioxide photocatalysts for environmental applications. Applied Catalysis B: Environmental. 2012;125:331-349.
29. Schneider J, Matsuoka M, Takeuchi M, Zhang J, Horiuchi Y, Anpo M, et al. Understanding TiO_2 Photocatalysis: Mechanisms and Materials. Chem Rev. 2014;114(19):9919-9986.
30. Açıkel YS, Göze B. Removal of Methyl Red, a cationic dye, Acid Blue 113, an anionic dye, from wastewaters using chitin and chitosan: influence of copper ions. Desalination and Water Treatment. 2017;73:289-300.
31. Nidheesh PV, Gandhimathi R, Ramesh ST. Degradation of dyes from aqueous solution by Fenton processes: a review. Environmental Science and Pollution Research. 2013;20(4):2099-2132.
32. Konstantinou IK, Albanis TA. TiO_2-assisted photocatalytic degradation of azo dyes in aqueous solution: kinetic and mechanistic investigations. Applied Catalysis B: Environmental. 2004;49(1):1-14.
33. Gaya UI, Abdullah AH. Heterogeneous photocatalytic degradation of organic contaminants over titanium dioxide: A review of fundamentals, progress and problems. Journal of Photochemistry and Photobiology C: Photochemistry Reviews. 2008;9(1):1-12.
34. Wang Y, Hong C-s. Effect of hydrogen peroxide, periodate and persulfate on photocatalysis of 2-chlorobiphenyl in aqueous TiO_2 suspensions. Water Res. 1999;33(9):2031-2036.

CC BY